Estimating the vertical variation of cloud droplet effective radius using multispectral near-infrared satellite measurements

Fu-Lung Chang and Zhanqing Li[1]

Earth System Science Interdisciplinary Center, University of Maryland, College Park, Maryland, USA

[1] This paper presents a satellite-based retrieval method for inferring the vertical variation of cloud droplet effective radius (DER) by utilizing multispectral near-infrared (NIR) measurements at 1.25, 1.65, 2.15, and 3.75 μm, available from the Moderate Resolution Imaging Spectrometer (MODIS) satellite observations. The method is based on the principle that these multispectral NIR measurements convey DER information from different heights within a cloud, which is sufficient to allow for the retrieval of a linear DER vertical profile. The method is applicable to low-level, nonprecipitating, stratiform clouds as their DER often increases monotonically from cloud bottom to cloud top. As such, an optimum linear DER profile can be derived by comparing multispectral NIR measurements to corresponding model values generated for a large set of linear DER profiles. The retrieval method was evaluated and compared to the conventional 3.7-μm retrieval method by applying both methods to some marine stratocumulus clouds with in situ observations of microphysical profiles. Capable of capturing the DER variation trend, the retrieved linear DER profiles showed large improvement over the conventional 3.75-μm retrievals. Mean differences between the linear DER retrievals and observed profiles were generally small for both cloud top and bottom (<1.0 μm), whereas the conventional retrievals are prone to systematic overestimation near cloud bottom. The sensitivities of the linear DER retrieval to various parameters, as well as the error analyses, were also investigated extensively. *INDEX TERMS:* 0320 Atmospheric Composition and Structure: Cloud physics and chemistry; 1704 History of Geophysics: Atmospheric sciences; 3359 Meteorology and Atmospheric Dynamics: Radiative processes; 3360 Meteorology and Atmospheric Dynamics: Remote sensing; 3394 Meteorology and Atmospheric Dynamics: Instruments and techniques; *KEYWORDS:* satellite retrieval, vertical profile, droplet radius

1. Introduction

[2] The dominant influence of clouds on Earth's radiation budget is well known. Even small changes in their abundance and distribution can alter Earth's climate more effectively than anticipated changes in trace gases, anthropogenic aerosols, and other factors affecting the global change [*Hartmann et al.*, 1992]. One of the important cloud microphysical parameters is the droplet effective radius (DER), which influence the Earth's climate through its effects on radiation balance, hydrological cycle, and cloud and climate feedbacks [*Charlson et al.*, 1987; *Albrecht*, 1989; *Twomey*, 1991; *Kiehl*, 1994; *Wielicki et al.*, 1995; *Stephens*, 1999]. Studies on the Earth's radiation budget have shown a large sensitivity to small changes in low-cloud droplet size [*Slingo*, 1990]. For example, Slingo estimated that a decrease in global, low-cloud, mean droplet size from 10 to 8 μm can induce an albedo cooling that would balance the greenhouse warming due to doubling atmospheric CO_2 concentration.

[3] However, cloud DER has been incorporated into climate models in an ad hoc manner, mainly due to the lack of systematic observations. Most climate models incorporate the DER information acquired from aircraft measurements at local experiments, usually limited to daytime, midlatitudes, and over land or coastal areas [*Slingo et al.*, 1982; *Stephens and Platt*, 1987; *Albrecht et al.*, 1988, 1995; *Twomey and Cocks*, 1989; *Rawlins and Foot*, 1990; *White et al.*, 1995; *Dong et al.*, 1997]. There is a dearth of observations concerning the DER vertical variability, a critical gap in the treatment of clouds in altering the heating rate and radiation budget in climate models. Thus routine satellite observations of clouds are required to gain a better knowledge on the vertical structure of cloud DER both at local and global scales and to understand its radiative effects on climate.

[4] Many studies on the retrieval of cloud DER from satellite observations have been devoted to the spectral measurement at the nominal 3.7 μm wavelength from the advanced very high resolution radiometer (AVHRR) [*Arking and Childs*, 1985; *Coakley et al.*, 1987; *Han et al.*, 1994; *Platnick and Twomey*, 1994; *Nakajima and Nakajima*,

[1]Also at Department of Meteorology, University of Maryland, College Park, Maryland, USA.

1995]. The fundamental basis of these retrieval methods is that the 3.7-μm spectral reflectance has a large dependence on DER. However, due to its large absorption by cloud droplets, the 3.7-μm reflectance is only susceptible to the DER variation near cloud top [*Platnick*, 2000]. As a result, the 3.7-μm retrieval is only valid for homogeneous DER vertical profiles. For inhomogeneous DER profiles, its retrieval may only represent a shallow layer near the cloud top and not the bulk property of the cloud.

[5] Since the advent of the Moderate Resolution Imaging Spectrometer (MODIS) from the Earth Observing System (EOS) [*King et al.*, 1992], retrieving DER vertical profiles has become feasible by using multispectral NIR measurements such as those at 1.24, 1.65, 2.15, and 3.75 μm. In a theoretic study on the vertical photon transport in a cloud layer at 1.6, 2.2, and 3.7 μm, *Platnick* [2000] investigated the photon multiscattering processes from infinitesimal layers to the overall reflectance contribution. Using analytic DER vertical profiles, he calculated the reflectance weighting functions from cloud top to bottom and showed significant differences among these wavelengths. Much of the weighting for 3.7 μm is confined to near cloud top, whereas the weighting at 1.6 μm spreads more evenly into the lower portion of the cloud. However, these weightings depend highly on the vertical variability of cloud DER and liquid water content, as well as the solar and viewing geometry. They cannot be determined without any a priori knowledge of the DER vertical profile.

[6] Since clouds formed by adiabatic or pseudo-adiabatic cooling often display a trend of near-linear increase in DER with height, an assumption of a linear DER profile should be valid. Among such category of clouds are a large number of low-level stratus and stratocumulus clouds observed in many experiments reviewed by *Miles et al.* [2000]. From satellite observations, these stratiform clouds, like marine stratocumulus, can cover large areas of hundred thousands of kilometers and last for several days [*Coakley and Baldwin*, 1984], which play an important role in determining the Earth radiation budget [*Hartmann et al.*, 1992]. They are capped by a temperature inversion due to both longwave radiative and droplet evaporative cooling at cloud top [*Nicholls and Turton*, 1986]. With very weak vertical motion, the growth of droplet size in stratiform clouds is mainly due to condensation rather than coalescence. As a result, for nonprecipitating and nonpollutant clouds, an increase in liquid water content with height in stratiform clouds is driven by an increase in droplet size rather than concentration. Yet, the increase is close to linear [*Miles et al.*, 2000]. In light of such linear DER variations, this study explores the potential of using coincident multispectral NIR satellite observations to retrieve a linear DER profile, which would otherwise be a formidable task.

[7] In section 2, the principle of the conventional cloud DER retrieval scheme is described. Section 3 presents some observational data sets containing typical profiles of cloud microphysics. They are used to illustrate and evaluate the proposed linear DER retrieval method. In section 4, the retrieval method is demonstrated through forward radiative transfer calculations and backward inversions. Section 5 presents error analyses due to various uncertainties with different combinations of the four MODIS NIR channels. The linear DER retrievals are also compared with those retrieved from the conventional method. A summary is given in section 6.

2. Conventional Cloud DER Retrieval Scheme

[8] Cloud optical depth (τ) and DER (r_e) are two primary cloud properties retrievable from remotely measured solar reflectance in visible and NIR channels, respectively. Solar reflectance by cloud is dominated by the scattering and absorbing properties of droplets [*Chandrasekhar*, 1960]. Figure 1 shows examples of cloud bidirectional reflectance (reflected radiance normalized by incident solar irradiance) calculated based on an adding-doubling radiative transfer model for various τ and r_e at five channels, i.e., 0.63, 1.24, 1.65, 2.15, and 3.75 μm. At the visible (0.63-μm) channel (Figure 1a), droplets are nonabsorbing. Photons transported within the cloud may undergo numerous scattering events deep into the cloud and still emerge from the cloud top. The visible reflectance is thus enhanced as cloud optical depth increases. The retrieval of cloud optical depth is fairly reliable even without accurate DER information [*Rossow et al.*, 1989].

[9] At the NIR channels (Figures 1b–1e), however, cloud droplets both scatter and absorb sunlight. Larger droplets absorb a larger fraction of radiance incident upon them than do smaller droplets and smaller droplets scatter more radiance than do larger droplets. Thus NIR reflectance decreases as droplet size increases. Since reflectance also increases with increasing cloud optical depth, the absorption causes the NIR reflectance to saturate at a certain optical depth level, where there is little chance that a photon can be transported beyond and still emerge from the cloud top without being absorbed. Such saturation occurs quicker if droplet absorption is stronger. For instance, 3.75-μm reflectance (Figure 1e) saturates fastest (at $\tau \approx 10$) and the larger the DER, the faster the saturation. Hence the DER retrieved based on a single NIR channel, like the conventional 3.75 μm, would rarely represent the bulk property of the whole cloud layer.

[10] Using aircraft reflectance measurements at 1.6 and 2.2 μm, respectively, *Nakajima and King* [1990] showed that the DER retrieved based on a single NIR channel is equivalent to the DER at a certain in-cloud optical depth level. Using two inhomogeneous DER vertical profiles, one from observations by *Albrecht et al.* [1988] and another from a linear DER model, they showed that the equivalent optical depth level varies with different liquid water content and DER profiles, which also highly depends on the NIR channel used. Overall, when comparing DER retrievals to in situ measurements, the former is generally larger than the latter by 25–40% [*Twomey and Cocks*, 1989; *Rawlins and Foot*, 1990; *Nakajima et al.*, 1991], while other studies showed better agreement [*Platnick and Valero*, 1995; *Han et al.*, 1995; *Nakajima and Nakajima*, 1995]. Such differences lead to concerns about the vertical variability of DER, as aircraft measurements may be taken from a cloud level that is different from the one inferred by remote sensing.

3. Cloud Microphysical Profiles and Simulated Reflectances

[11] Cloud liquid water content, DER, and dispersion (σ) of the lognormal size distribution observed from several
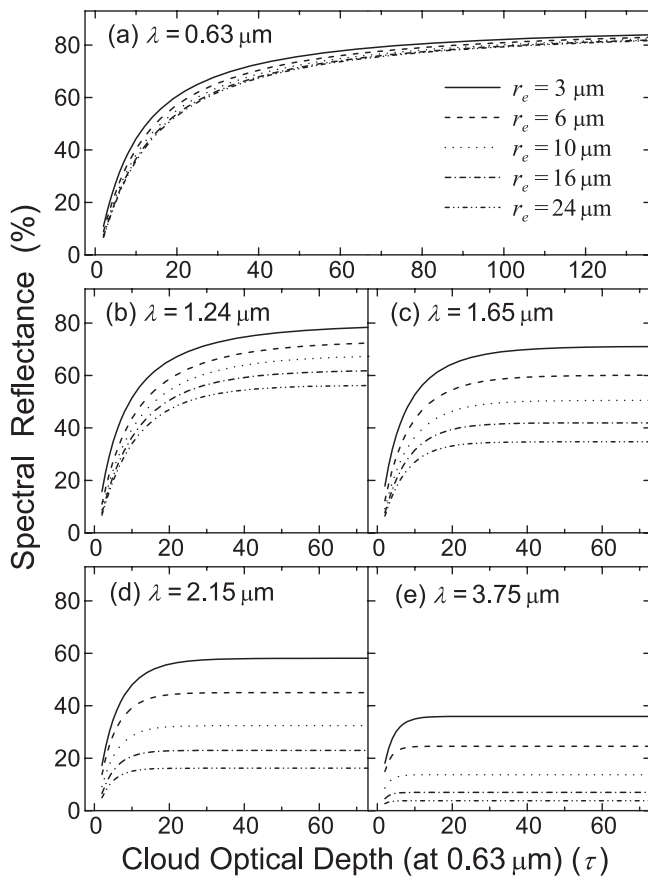
Figure 1. The dependence of the spectral reflectances on cloud optical depth and DER for λ = (a) 0.63 μm, (b) 1.24 μm, (c) 1.65 μm, (d) 2.15 μm, and (e) 3.75 μm. The reflectances are obtained for $(\theta_0, \theta, \phi-\phi_0)$ = (60.0°, 7.2°, 0.0°) with r_e = 3, 6, 10, 16, and 24 μm.

size distribution for Δh = 200 m (solid curve), 600 m (dashed curve), and 1600 m (dotted curve), respectively. The vertical axis is given in terms of fractional cloud geometrical depth, h', given by

$$h' = (h - h_T)/(h_B - h_T), \qquad (1)$$

where $h' = 0$ denotes the cloud top (h_T) and $h' = 1$ denotes cloud bottom (h_B). Since the microphysical vertical profiles for Δh = 1600 m are composed of 160 layers, they exhibit more fluctuations than do the profiles for Δh = 200 m, which are only composed of 20 layers.

4. Retrievals of the Linear DER Profile

[13] The retrieval method employs a lookup table technique that determines the DER profile by comparing observed multispectral NIR reflectances with model precalculated
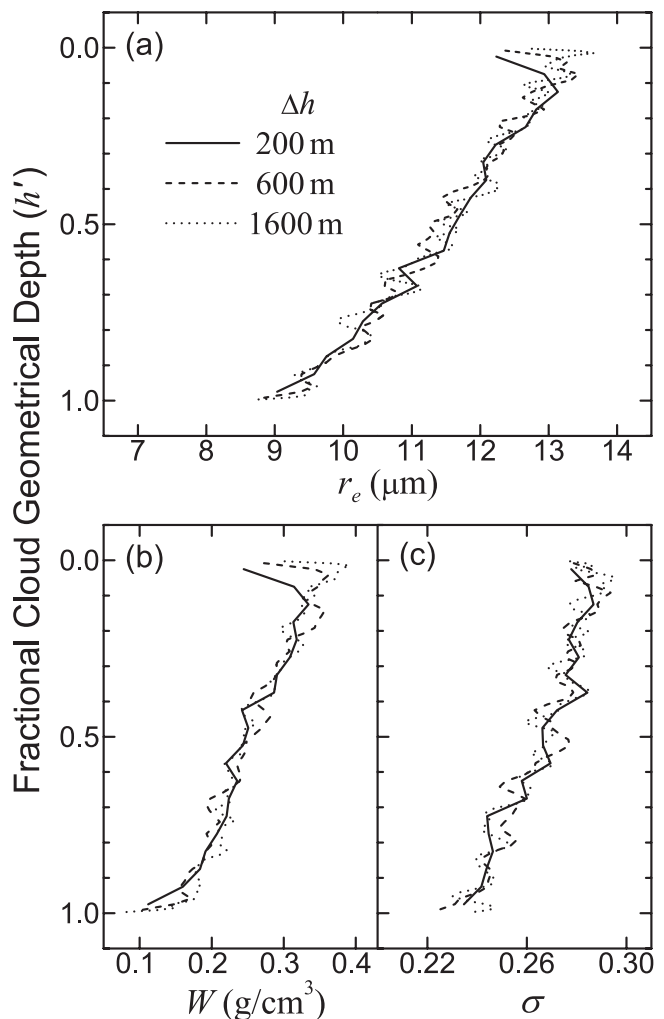
marine stratocumulus field experiments are employed to illustrate and evaluate the retrieval method. The performance of the proposed linear DER retrieval method is evaluated with reference to (1) real DER profiles obtained from in situ measurements and (2) retrieved DER by the conventional method. A typical low-level marine stratocumulus cloud observed during the Atlantic Stratocumulus Transition Experiment (ASTEX) [*Albrecht et al.*, 1995] was used to demonstrate the retrieval methodology. The retrieval performance was then assessed by several case studies of marine stratocumulus clouds as documented by *Miles et al.* [2000, Table 1], which contains in situ aircraft measurements of microphysical profiles. An adding-doubling radiative transfer code [*Chang*, 1997] was applied to simulate satellite reflectance measurements for the observed cases. Since cloud microphysical properties were reported at three vertical levels, i.e., near cloud top, midlevel, and cloud bottom, respectively, these properties were interpolated linearly and superimposed by randomly generated noise. Cloud optical depths were then calculated for every 10-m geometrical thickness for an overall cloud vertical thickness (Δh) ranging from a hundred to a couple thousand meters.

[12] Figure 2 illustrates three examples of the simulated vertical profiles of DER (Figure 2a), liquid water content (Figure 2b), and dispersion (Figure 2c) of the lognormal

Figure 2. Vertical profiles of (a) cloud DER, (b) liquid water content, and (c) the dispersion (σ) of the lognormal size distribution that were simulated for three cloud geometrical thicknesses of 200, 600, and 1600 m. These profiles were simulated based on the observed values measured at the top, middle, and bottom of a marine stratocumulus cloud during ASTEX.

tables of reflectance. The method includes two major steps: (1) forward radiative transfer calculations and (2) the inversion retrieval procedure.

4.1. Forward Radiative Transfer Calculations

[14] The purpose of forward radiative transfer calculations is to generate a large set of reflectance lookup tables at 0.63, 1.24, 1.65, 2.15, and 3.75 μm. Radiative transfer calculations were conducted for various conditions of cloud optical depths and linear DER profile. The DER profile is assumed to be a linear function of in-cloud optical depth (τ'), which is given by

$$r_e(\tau') = r_{e1} + (r_{e2} - r_{e1})\frac{\tau'}{\tau_{total}}, \qquad (2)$$

where τ_{total} is the total cloud optical depth at 0.63-μm and r_{e1} and r_{e2} are two prescribed boundary conditions at cloud top ($\tau' = 0$) and cloud bottom ($\tau' = \tau$), respectively.

[15] Using such a linear DER profile, reflectances were calculated by employing the adding-doubling radiative transfer routine with many superimposed infinitesimal cloud layers [*Platnick*, 2001a]. For speedy radiative transfer calculations while maintaining good accuracy, the adding-doubling calculations adopted variable optical depth layers to deal with the vertically inhomogeneous cloud model. The superimposition starts with very thin optical depth layers near the cloud top and then adopts progressively thicker layers toward the cloud bottom. The intervals of cloud optical depth adopted are $\Delta\tau_k = 0.25$ for $k = 1-8$ ($\tau_{total} = 2$ at $k = 8$), $\Delta\tau_k = 0.5$ for $k = 9-16$ ($\tau_{total} = 6$ at $k = 16$), $\Delta\tau_k = 1.0$ for $k = 17-30$ ($\tau_{total} = 20$ at $k = 30$), $\Delta\tau_k = 2.0$ for $k = 31-44$ ($\tau_{total} = 48$ at $k = 44$), and $\Delta\tau_k = 4.0$ for $k = 45-56$ ($\tau_{total} = 96$ at $k = 56$), where k denotes the kth layer from cloud top downward in the adding procedures. The lookup table reflectances (hereinafter denoted by L_λ) for $\lambda = 0.63$, 1.24, 1.65, 2.15, and 3.75 μm were thus generated for discrete τ_{total} = 4, 5, 6...112.

[16] To encompass the range of DER profiles, calculations were made for a combination of $r_{e1} = 3.0, 3.1, 3.2...$ 30 μm and $r_{e2} = 3.0, 3.2, 3.4...$ 30 μm, respectively. For each linear DER profile, the dispersion of the lognormal size distribution was set to be a constant, but using different values, namely, $\sigma = 0.17, 0.20, 0.23... 0.62$. Note that the droplet scattering and absorbing properties were calculated at 0.2-μm intervals between 3.0–30 μm, based on Mie theory and refractive indices for 0.63, 1.24, and 1.65 μm from *Hale and Querry* [1973] and 2.15 and 3.75 μm from *Downing and Williams* [1975]. The DER for each thin layer ($\Delta\tau_k$) was approximated by a constant equivalent to the value at the center of that layer. The droplet scattering and absorbing properties were then approximated by linear interpolation according to the database of the 0.2-μm DER grids.

[17] Since the adding-doubling radiative transfer calculations are based on the plane-parallel assumption, the retrieval method is better applied to low-level, stratiform clouds with uniform cloud tops [*Chang et al.*, 2000]. Here, the retrieval focuses on near-nadir observations to avoid the dependence on satellite viewing zenith (θ) and azimuth ($\phi-\phi_0$) angles. Also, the solar zenith angle (θ_0) is restricted to <60° to reduce the shadow effect due to uneven cloud
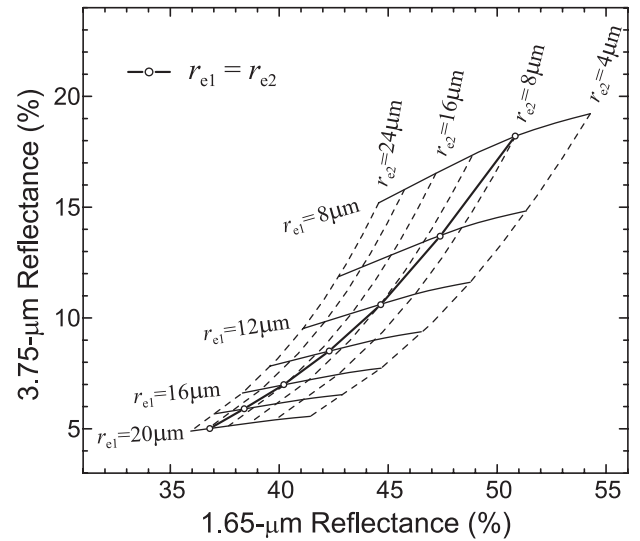

Figure 3. The NIR reflectance dependence on r_{e1} and r_{e2} at 3.75 μm versus 1.6 μm. The reflectances are obtained for $(\theta_0, \theta, \phi-\phi_0) = (60.0°, 7.2°, 0.0°)$ and $\tau_{total} = 20$.

top structure [*Loeb and Coakley*, 1998]. As such, reflectance is simply a function of four variables: $\tau_{total}, r_{e1}, r_{e2}$, and σ, though it also varies with θ_0, θ, and $\phi-\phi_0$.

[18] Figure 3 shows NIR reflectances $L_\lambda(\tau_{total}; r_{e1}, r_{e2}, \sigma)$ at 1.65 μm versus 3.75 μm, which were calculated using different r_{e1} and r_{e2} for the linear DER profile and a constant $\sigma = 0.35$. It is seen that the NIR reflectances depend on both the cloud-top r_{e1} and the linear variance toward r_{e2}. Since the larger the DER the more the absorption, the reflectance dependence on r_{e2} decreases as r_{e1} increases. Also, since the longer the wavelength the faster the reflectance saturation, the 3.75-μm reflectance displays much less sensitivity to variation in r_{e2}, as opposed to the 1.65-μm reflectance. Such reflectance dependence on both r_{e1} and r_{e2} lays the foundation for retrieving the linear DER profile.

4.2. Retrieval Procedure

[19] The proposed linear DER retrieval method, like conventional ones, follows an iterative procedure to retrieve τ_{total} from the visible reflectance measurement at 0.63-μm and a linear DER profile from multi-NIR reflectance measurements at 1.24, 1.65, 2.15 and 3.75 μm. The specific retrieval steps are described as follows.

[20] The first step is to retrieve τ_{total} by interpolating a 0.63-μm reflectance observation using a lookup table with specified r_{e1}, r_{e2}, and σ. This step is similar to the conventional approach in DER retrieval [*Han et al.*, 1994; *Platnick and Valero*, 1995; *Nakajima and Nakajima*, 1995], except that the DER is described by two parameters, r_{e1} and r_{e2}. At the first iteration, an initial guess of the linear DER profile is necessary, e.g., $r_{e1} = r_{e2} = 10$ μm and $\sigma = 0.35$. For the following iterations, retrievals of r_{e1} and r_{e2} are updated.

[21] The second step is to retrieve an optimum linear DER profile that is best fit to the four NIR reflectance observations at 1.24, 1.65, 2.15 and 3.75 μm. The optimum linear DER profile is determined by searching for a mini-
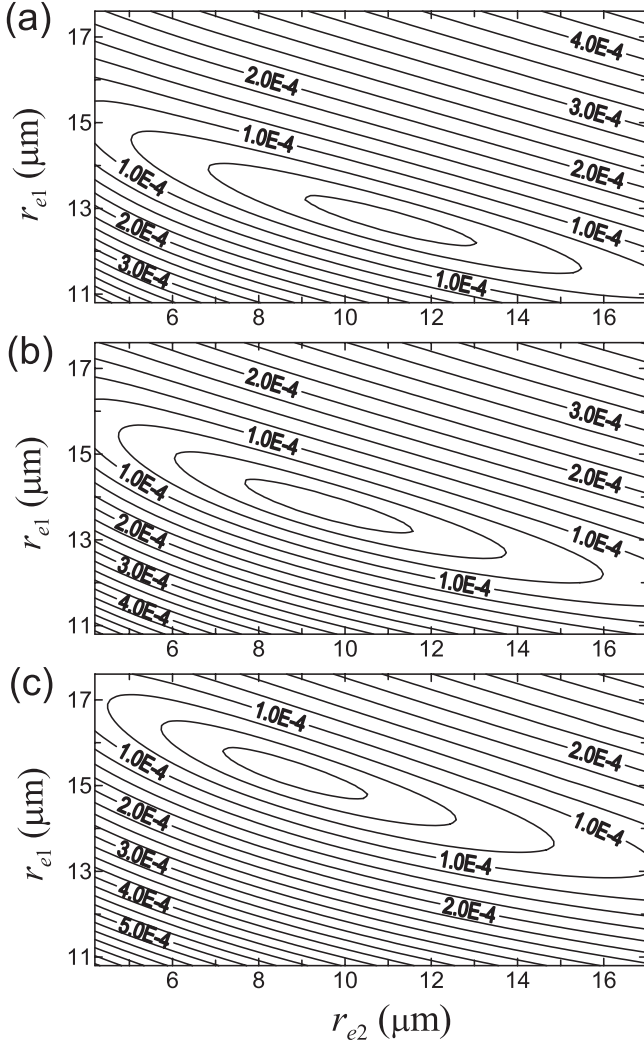
Figure 4. Contour plots showing the values of the χ^2 statistics calculated for various r_{e1} and r_{e2} with σ = (a) 0.20, (b) 0.35, and (c) 0.50. Results are obtained for the cloud case of Δh = 600 m shown in Figure 2 and $(\theta_0, \theta, \phi - \phi_0)$ = $(60.0°, 7.2°, 0.0°)$.

mum least squares variance χ^2 between observed and modeled multispectral NIR reflectances, which is defined by

$$\chi^2(\tau_{total}; r_{e1}, r_{e2}, \sigma) = \frac{\sum_{m=1}^{M} [R_m - L_m(\tau_{total}; r_{e1}, r_{e2}, \sigma)]^2 w_m}{\sum_{m=1}^{M} w_m}, \quad (3)$$

where R_m and L_m denote the observed and modeled reflectances, respectively, at the mth NIR channel, w_m is the weighting factor, and $M = 4$ is the total number of NIR channels. The optimum linear DER profile is thus given by the r_{e1} and r_{e2} corresponding to the minimum χ^2.

[22] The next step is to repeat steps 1 and 2 by using updated retrievals of τ_{total}, r_{e1} and r_{e2}. An iterative procedure is followed until the retrievals converge to stable values, which are usually achieved within 2-3 iterations. It

is worth noting that in this modeling exercise, it is assumed that the thermal emission is removed from satellite observations at the 3.75-μm channel. The removal procedure has been addressed in numerous studies that invoke thermal infrared measurements made nominally at 11 μm [*Han et al.*, 1994; *Platnick and Valero*, 1995; *Nakajima and Nakajima*, 1995]. The removal is more reliable for optically thick clouds ($\tau_{total} > 10$) that are opaque at the two channels. Improved instrument calibrations of MODIS and its spectral consistency help enhance the accuracy of subtraction of the 3.75-μm emission.

[23] Figure 4 shows a contour plot of the χ^2 values obtained for the case of Δh = 600 m shown in Figure 2 by using different values of σ (0.20, 0.35 and 0.50). The χ^2 values were obtained by using equal weights (w_m = 25%) for all NIR channels and τ_{total} = 20.51 retrieved from the 0.63-μm channel. It is seen that the values of χ^2 converge to a singular minima in all three sub-panels. Table 1 lists the minimum χ^2 and corresponding retrievals of τ_{total}, r_{e1}, and r_{e2} obtained using different σ values for the case shown in Figure 4. For instance, a minimum $\chi^2 = 2.51 \times 10^{-6}$ obtained with σ = 0.35 occurs at r_{e1} = 13.8 μm and r_{e2} = 9.4 μm, which are in agreement with the truth input of r_{e1} = 13.4 μm and r_{e2} = 9.5 μm. While such a convergence to a singular minimum can always be achieved at near-nadir viewing conditions, nonsingular solutions may occur at other scattering and viewing conditions due to the somewhat ambiguous dependence of NIR reflectances on r_e [*Nakajima and King*, 1990]. In particular, in the backward scattering directions with a moderate large viewing zenith angle, the reflectances at 1.65, 2.15 and 3.75 μm all exhibit certain dual dependence on r_e, leading to several local minima in the χ^2 domain, posing a considerable difficulty or failure for the retrieval.

[24] In principle, an optimal solution of a constant σ profile for the linear DER retrieval may be determined by searching for an overall minimum of χ^2 in terms of all four variables, i.e., τ_{total}, r_{e1}, r_{e2} and σ. As shown in Table 1, the minimum χ^2 obtained with different σ show an overall minimum of 2.35×10^{-6} at σ = 0.29. However, the optimal determination of σ relies largely on the accuracy in the retrievals of τ_{total}, r_{e1}, and r_{e2}. Small uncertainties in the retrievals of τ_{total}, r_{e1}, and r_{e2} can incur large errors in the determination of σ. Thus, for operational applications, retrieving σ seems impractical. Fortunately, as shown in

Table 1. Retrievals of τ_{total}, r_{e1}, and r_{e2} and Corresponding Minimum χ^2 for Various σ

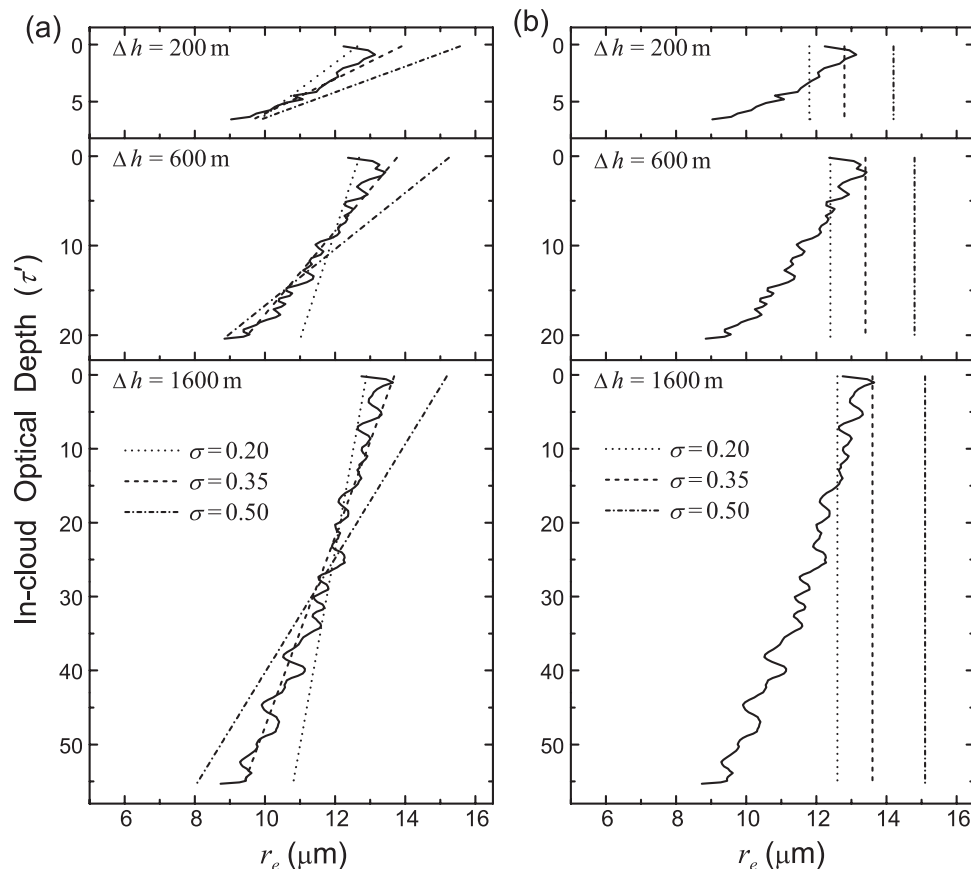| σ	τ_{total}	r_{e1}, μm	r_{e2}, μm	χ^2, $\times 10^{-6}$
0.20	20.61	12.7	11.0	10.60
0.23	20.58	12.9	10.6	7.57
0.26	20.57	13.0	10.4	4.51
0.29	20.55	13.3	10.0	2.43
0.32	20.48	13.5	9.8	2.46
0.35	20.45	13.8	9.4	2.51
0.38	20.38	14.0	9.4	2.83
0.41	20.32	14.3	9.2	3.25
0.44	20.25	14.6	9.0	3.61
0.47	20.20	15.0	8.8	5.14
0.50	20.14	15.3	8.8	6.25
0.53	20.06	15.6	9.0	6.82
0.56	19.99	16.0	9.0	8.27

Figure 5. Comparisons between the observed (solid) and retrieved DER profiles using (a) the linear DER retrieval method and (b) conventional 3.75-μm method for the three cloud cases shown in Figure 2. Three different DER profiles were retrieved using σ = 0.20 (dashed), 0.35 (dotted) and 0.50 (dash-dotted).

later error analyses, using a constant σ in the range of 0.35–0.40 generally produces good agreement between the retrievals and observations.

[25] The linear DER retrievals are also compared with the conventional retrievals using a single 3.75-μm channel. Figure 5 shows the retrievals obtained from both methods for the three cloud cases shown in Figure 2 (i.e., $\Delta h = 200$ m, 600 m, and 1600 m with τ_{total} = 6.65, 20.51 and 55.41 respectively), which are plotted against the observed DER profiles. As the retrievals are obtained using σ = 0.20, 0.35, and 0.50, respectively, both methods show dependence on the selection of σ. Nonetheless, the linear DER retrievals (Figure 5a) portray a significantly better trend than do the retrievals with the single 3.75-μm channel (Figure 5b). The observed DER profile falls within the two linear DER retrievals with σ = 0.20 and 0.35, whereas the 3.75-μm channel retrievals fail to provide any information on the DER vertical variability. The latter also gives rise to biased estimates with respect to column mean and cloud-bottom DER. The retrieval may be either equivalent to the DER at a deeper cloud level or completely different from the entire DER profile, contingent upon the difference between the assumed and actual σ values.

[26] Besides, the linear DER retrievals shown in Figure 5a are subject to change with the weights (w_m) applied to the multiple NIR channels. In general, putting more weight on

the shorter wavelengths (less absorption) lead to linear DER retrievals that were more capable of representing the full DER profile. Also, the more weight on the shorter wavelengths, the better the retrieval for large τ_{total}. On the other hand, putting more weight on the longer wavelengths (more absorption) improves the retrieval near cloud top, at the expense of a large bias near the cloud bottom.

5. Error Analyses

[27] To evaluate potential uncertainties in the retrieval of DER, the proposed inversion method was applied to several marine stratocumulus cloud data sets consisting of observed vertical profiles of cloud DER, liquid water content, and σ. The microphysical measurements were obtained from various experiments described by *Albrecht et al.* [1995], *Duda et al.* [1991], *Duynkerke et al.* [1995], *Martin et al.* [1994] (three cases), *Nicholls* [1984], *Ryan et al.* [1972], and *Stephens and Platt* [1987] (nonprecipitating case). They were documented by *Miles et al.* [2000, Table 1]. Cloud liquid water content ranges roughly between 0.15–0.59 g m^{-3} at cloud top and 0.01–0.16 g m^{-3} at cloud bottom. The DER ranges roughly between 8–14 μm at cloud top and 4–10 μm at cloud bottom and σ ranges between 0.23–0.54 at cloud top and 0.24–0.74 at cloud bottom. The geometrical thickness ranges from 100 m to 2000 m with corresponding τ_{total} from
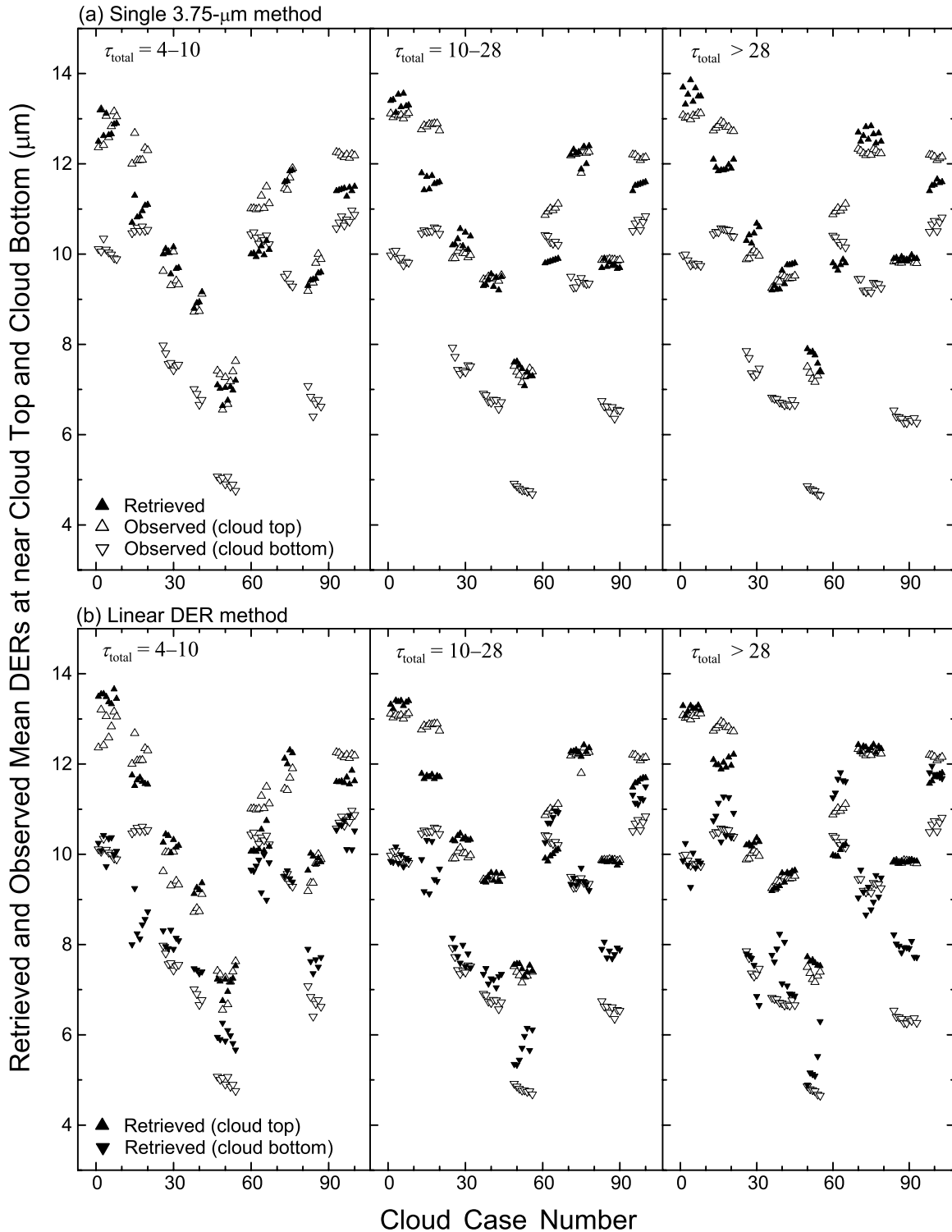
Figure 6. Case-by-case comparisons between the observed (open) and retrieved (solid) mean DERs for a) conventional 3.75-μm and b) linear DER retrieval methods. Results are shown separately for $\tau_{total} = 4$–10, 10–28, and >28. The cloud-top (triangle) and cloud-bottom (inverted triangle) means are obtained by averaging over the 10–20th and 80–90th percentiles of the profile, respectively.

about 4 to 100. These profiles were used to simulate the MODIS spectral reflectance measurements.

[28] Both the conventional 3.75-μm and linear DER retrieval methods were applied to the simulated reflectances for the observed cloud cases. Mean DERs from the retrieved and observed profiles were compared at both cloud top and bottom, which were calculated by averaging the DER profiles in the 10–20th (i.e., cloud top) and 80–90th (i.e., cloud bottom) percentiles of optical depth intervals, respectively. The 0–10th and 90–100th percentiles were avoided
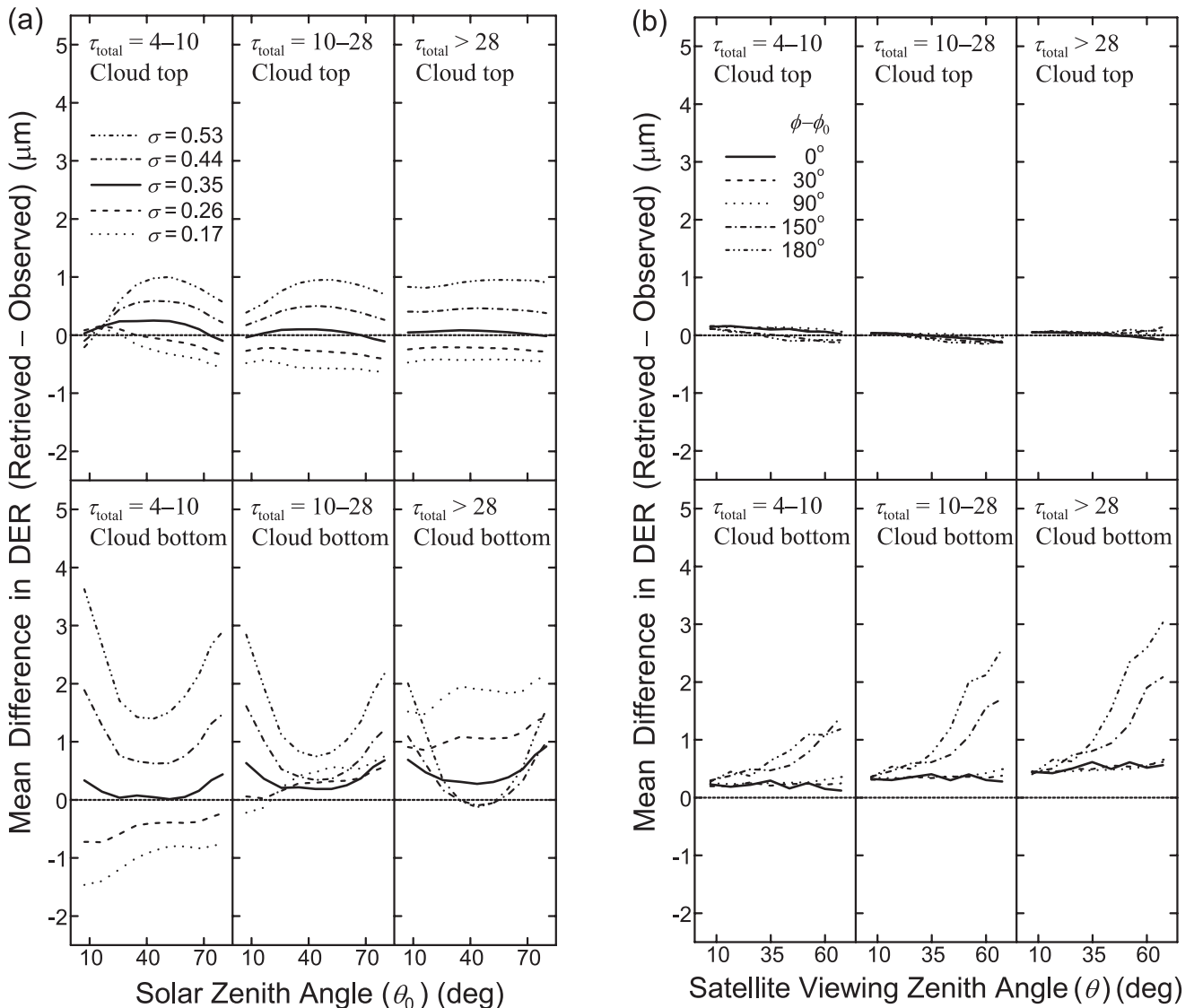
Figure 7. (a) The dependence of the mean DER difference (retrieved minus observed) on θ_0 for the linear DER retrievals with equal weights on the four NIR channels. The retrievals were made for near-nadir reflectances using five $\sigma = 0.17$, 0.26, 0.35, 0.44, and 0.53. Results are shown for (top) cloud top and (bottom) cloud bottom with $\tau_{total} = 4-10$, 10–28, and >28. (b) Similar to Figure 7a, except for the dependence of the mean DER difference on θ. Results are shown for $\phi - \phi_0 = 0°$, 30°, 90°, 150°, and 180° with $\theta_0 = 60.0°$ and $\sigma = 0.35$.

as the DER often changes drastically at the very top and bottom of a cloud due to mixing with ambient air.

[29] Figure 6 shows case-to-case comparisons of the observed and retrieved cloud-top and cloud-bottom mean DERs for the conventional 3.75-μm method (Figure 6a) and the linear DER retrieval method (Figure 6b) using $\sigma = 0.35$ and equal weights for four NIR channels. The comparisons were grouped into $\tau_{total} = 4-10$, 10–28, and >28. In each panel, the clustering of points is due to applying different assumed cloud vertical thickness to the cloud cases from *Miles et al.* [2000]. As expected, the DER retrievals from the conventional 3.75-μm method match well with the observed means at the cloud top, but are considerably larger than the values near cloud bottom. By contrast, the linear DER retrievals show good agreement at both cloud top and bottom.

In general, the linear DER retrievals for moderate τ_{total} (10–28) exhibit better agreement in cloud-bottom DER than those for smaller (<10) or larger (>28) τ_{total}. This is because for smaller τ_{total}, NIR reflectance depends more strongly on τ_{total} (as shown in Figure 1), rendering a larger uncertainty. Yet, for larger τ_{total}, clouds tend to have a better defined linear DER. Of course, this would not be the case if DER has a more complex, nonlinear vertical profile. Overall, the comparisons attest that the new retrieval approach is promising, especially with respect to the conventional method.

[30] Nevertheless, the linear DER retrievals were unsuccessful for certain cases. For the cases near index number 15, the underestimated retrievals originated from a discrepancy in σ between observed (0.46 at cloud top and 0.74 at cloud bottom) and assumed (0.35) values. For the cases near

index number 65, the observed DER profiles have a non-linear variation that generally increases in the upper half but decreases in the lower half. Such split trends negate the linear assumption and cause biases in the linear DER retrieval, where the retrieved DERs are reversed for the cloud-top and cloud-bottom means. For the cases near number 100, they have a near-constant DER profile for the upper half of the cloud and then a decrease toward cloud bottom for the lower half, so that the DER retrievals for both cloud top and bottom are nearly identical since they overlap on each other.

[31] The linear DER retrievals are also examined for dependence on solar incident and viewing geometries. Figure 7a shows the dependence of the mean DER differences (retrieved minus observed) on θ_0 for the retrievals made at near-nadir viewing angle with equal weights on the NIR channels. The dependence is shown for the retrievals obtained using five different constant σ (0.17, 0.26, 0.35, 0.44, and 0.53), respectively. The mean DER difference for the cloud top shows little dependence on θ_0 for $\tau_{total} > 10$. For varying σ from 0.17 to 0.53, the mean retrieved DER generally differs by about 1.0–1.5 μm. However, for the cloud bottom, the mean differences show a larger dependence on both θ_0 and σ. The dependence on σ is also larger at both ends of the solar zenith angles for $\tau_{total} < 10$. It is interesting to note that using $\sigma = 0.35–0.40$ generally produce the mean differences that are close to zero at cloud top and less than 0.5 μm at cloud bottom for the median range θ_0. The RMS errors of these mean differences are usually on the order of 1.0 μm. Using commonly assumed $\sigma = 0.35$, the retrievals are in good agreement at both cloud top and bottom in terms of their magnitude of the differences and dependence on θ_0.

[32] Figure 7b shows the mean differences as a function of θ in two forward scattering directions ($\phi - \phi_0 = 0°$ and 30°), one side scattering direction ($\phi - \phi_0 = 90°$), and two backward scattering directions ($\phi - \phi_0 = 150°$ and 180°) for the retrievals at $\theta_0 = 60°$ using $\sigma = 0.35$ and equal weights. It is seen that the mean differences are generally small (<1.0 μm) at all viewing directions, except for the backward scattering directions at $\phi - \phi_0 = 150°$ and 180° with viewing zenith angles >30°. As mentioned earlier, such large differences in the backward scattering directions stem from the nonsingular dependence of the NIR reflectance on DER, leading to the ambiguous linear DER retrievals.

[33] The effects of solar and viewing geometry presented in Figure 7 are used here to examine the self-consistency within the retrieval model itself. While cloud inhomogeneity may also cause an angular dependence in the retrieval, it is difficult to quantify the effects without detailed measurements from both outside and within the cloud. In a vertically inhomogeneous, plane-parallel cloud layer (as used in this study), *Platnick* [2000, 2001b] examined the photon vertical and horizontal transport processes at 0.66, 1.6, 2.2, and 3.7 μm and found good agreements in azimuth-averaged reflectances computed by an adding-doubling model and a Monte Carlo code. He also showed that photon horizontal transport at NIR wavelengths were limited to a few tens of optical depth unit for 1.6 μm and a few optical depth units for 3.7 μm due to droplet absorption. The effect of cloud horizontal inhomogeneity should be less significant for the more absorbing NIR wavelengths.
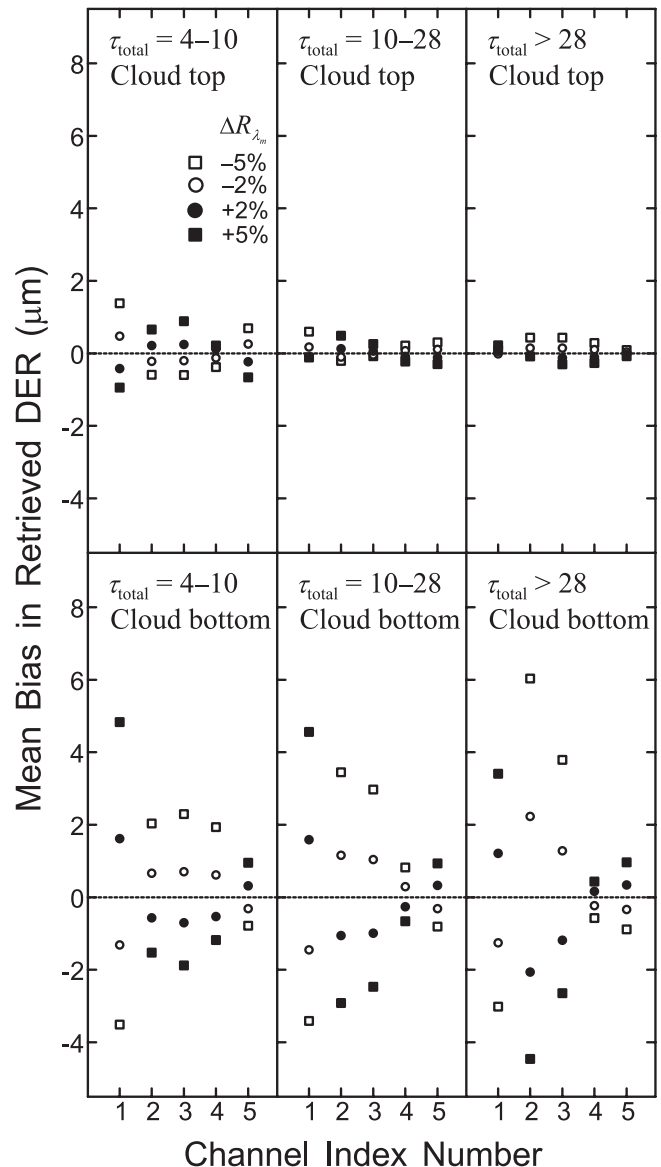

Figure 8. The dependence of the mean biases in linear DER retrievals on the reflectance error ($\Delta R_{\lambda m}$) at each spectral channel. The mean biases are shown for relative errors of +5% (solid square), +2% (solid circle), −2% (open circle) and −5% (open square), respectively, for the near-nadir retrievals with $\theta_0 = 60.0°$ and $\sigma = 0.35$. Channel index numbers 1–5 are explained in the text.

[34] On the other hand, using AVHRR 0.63-μm reflectance measurements made over marine stratocumulus clouds, *Loeb and Coakley* [1998] examined τ_{total} inferred by a plane-parallel model and found dependence on both the solar and viewing zenith angles. The viewing angle dependence may be caused by less reflectance at larger viewing angles due to hidden broken cloud fields or finite boundaries of the stratocumulus, which were misidentified as overcast fields. The dependence on θ_0 was most significant at very large θ_0, which was attributed to the shadow effects from the bumpy cloud-top structure for a slant incident angle.

[35] Mean biases in the linear DER retrievals due to the uncertainty in individual reflectance measurements are shown in Figure 8 for nadir viewing angles with $\theta_0 = 60°$, $\sigma = 0.35$, and equal weights. The bias error was estimated by preassigning an error ($\Delta R_{\lambda m}$) in a single channel denoted by the index numbers, 1 for 0.63 μm, 2 for 1.24 μm, and so forth. Shown in the figure are the results for four different relative uncertainties ($\Delta R_{\lambda m}$ = +5%, +2%, −2%, and −5%). The DER retrievals for cloud top are relatively insensitive to uncertainties in reflectance measurements, whereas the retrievals for cloud bottom are subject to larger biases. Since the retrieval of cloud-bottom DER relies heavily on

Table 2. Index Numbers and Normalized Weights Used in the Four NIR Channels

Index	Normalized Weights, %			
	1.24 μm	1.65 μm	2.15 μm	3.75 μm
1	50	50	0	0
2	50	40	10	0
3	33	34	33	0
4	10	40	50	0
5	0	50	50	0
6	0	50	40	10
7	0	33	34	33
8	0	10	40	50
9	0	0	50	50

the shorter NIR channels, they are more sensitive to the reflectance errors in channels 2 (1.24 μm) and 3 (1.65 μm). Large biases can also arise from errors in channel 1 (0.63 μm) for the retrieval of τ_{total} but are opposite in sign to the biases of channels 2 and 3.

[36] Instrument calibration can be a major source of uncertainty. For MODIS data, the uncertainty and spectral consistency are estimated to be <1−2% [*King et al.*, 1992]. Another source of uncertainty is the modeling of atmospheric absorption and surface reflection. Poor estimates of these effects may contribute to an uncertainty of several percents in instantaneous reflectance calculations [*Chang et al.*, 2000]. Hence a better knowledge on atmospheric and surface conditions warrants more accurate retrieval. Besides, uncertainty may also arise from the subtraction of the 3.75-μm emission [*Han et al.*, 1994; *Platnick and Valero*, 1995; *Nakajima and Nakajima*, 1995], which may be more significant for the conventional retrieval that depends solely on a single 3.75 μm. Since the subtraction requires additional infrared measurements such as 11 μm, the spectral consistency and accurate calibrations of the instruments are thus essential.

[37] Figure 9 shows the mean differences of retrieved minus observed DERs (solid line) using different combinations and weightings of the multiple NIR channels as indicated by the index numbers 1 to 9, which are listed in Table 2. Again, they are for near-nadir views with $\theta_0 = 60°$ and $\sigma = 0.35$. The mean differences exhibit a certain dependence on the choice of channels and weights, but are generally weak (<1 μm). The dependence generally increases with increasing viewing angle. In addition, the figure also shows the mean differences obtained by assigning an error to all five channels with ΔR_λ = +5%, +2%, −2%, and −5%, respectively. Similar to Figure 8, the biases are small for the cloud top, but somewhat smaller for the cloud bottom, due to cancellation of errors from individual channels.
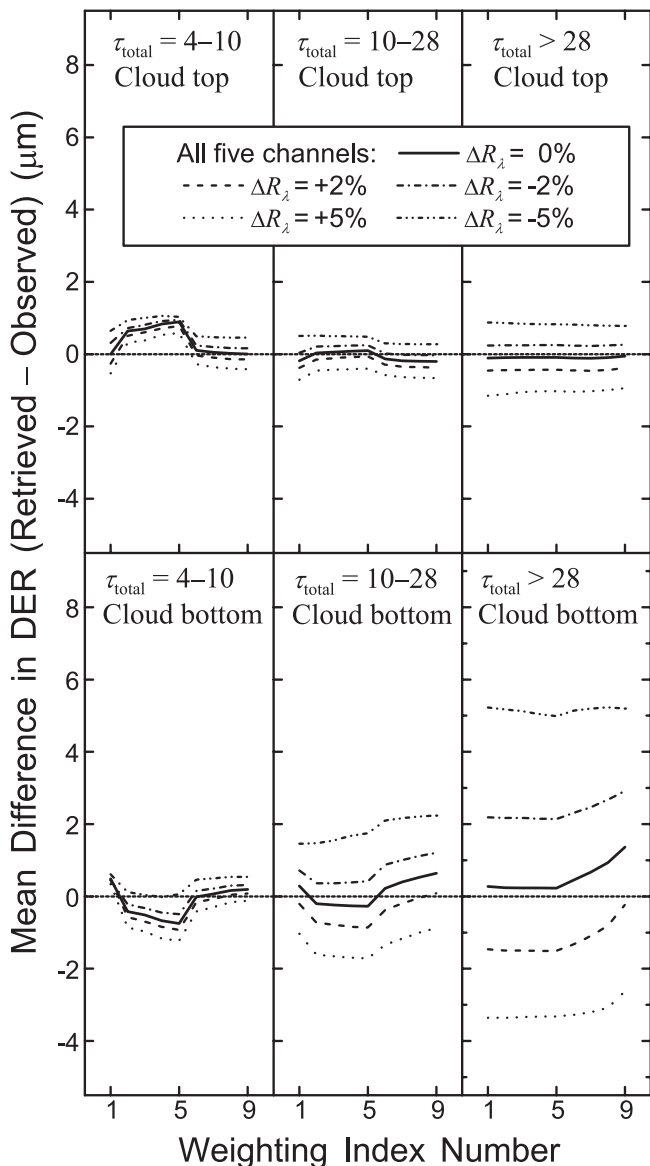

Figure 9. The dependence of the mean DER differences (retrieved minus observed) on the different selection of NIR channels and weights, as shown in solid curves. Results are also compared by assuming reflectance errors of ΔR_λ = +5% (dotted), +2% (dashed), −2% (dash-dotted), and −5% (dash-dot-dotted) in all five channels. Index numbers representing different weights are given in Table 2. Results are shown for near-nadir reflectances with $\theta_0 = 60.0°$ and $\sigma = 0.35$.

6. Summary

[38] Given its significant influence on the radiative transfer and hydrological cycle, cloud droplet size is critically needed for climate modeling. So far, limited information has been gained primarily through a handful of field campaigns. Satellite remote sensing techniques have been employed, but their retrievals are limited to the uppermost cloud layer. This paper presents a new retrieval method for estimating the vertical variations of cloud droplet effective radius (DER) utilizing multispectral

near-infrared (NIR) reflectance measurements at 1.24, 1.65, 2.15, and 3.75 μm, which are available from the Moderate Resolution Imaging Spectrometer (MODIS) satellite observations.

[39] The principle of the retrieval method lies in that NIR reflectances at different wavelengths have variable sensitivity to DER at different levels inside a cloud layer. As such, one may extract some information on the vertical distribution of DER by using multispectral NIR reflectance measurements. Since the DER for nonprecipitating stratus and stratocumulus clouds formed by adiabatic process often show near linear increase with height, this study explores the utility of MODIS multichannel NIR measurements to retrieve a linear DER profile. In general, an optimum linear DER profile can be retrieved by fitting the multispectral NIR reflectance measurements with model calculations, which captures the trend of the DER vertical variation. This is in contrast to the conventional retrievals using a single 3.75-μm channel that represent only the uppermost cloud portion with a tendency to overestimate the cloud-bottom DER.

[40] The method is most effective for near-nadir observations made over uniform stratiform clouds with DER varying linearly with height at relatively small solar zenith angles. Violation of any of the assumptions invoked in the retrieval method, such as a nonlinear variation of DER, cloud heterogeneity, large solar and viewing zenith angles, can undermine the retrieval. Errors and sensitivities of the retrievals resulting from various uncertainties were investigated. It was found that uncertainties in reflectance measurements have a relatively small impact on cloud-top DER retrievals, whereas the cloud-bottom retrievals are more susceptible to the uncertainties. Accurate retrievals of the linear DER profile thus hinge on the quality and consistency of multispectral NIR reflectance measurements. The required measurement accuracy and consistency is 1–2%, which appear to be satisfied by the data.

References

Albrecht, B. A., Aerosols, cloud microphysics, and fractional cloudiness, *Science*, *245*, 1227–1230, 1989.

Albrecht, B. A., D. A. Randall, and S. Nicholls, Observations of marine stratocumulus clouds during FIRE, *Bull. Am. Meteorol. Soc.*, *69*, 618–626, 1988.

Albrecht, B. A., C. S. Bretherton, D. Johnson, W. H. Schubert, and A. S. Frisch, The Atlantic Stratocumulus Transition Experiment—ASTEX, *Bull. Am. Meteorol. Soc.*, *76*, 889–904, 1995.

Arking, A., and J. D. Childs, The retrieval of cloud cover parameters from multi-spectral satellite images, *J. Clim. Appl. Meteorol.*, *24*, 322–333, 1985.

Chandrasekhar, S., *Radiative Transfer*, 393 pp., Dover, Mineola, N. Y., 1960.

Chang, F.-L., Properties of low-level marine clouds as deduced from AVHRR satellite observations, Ph.D. dissertation, 335 pp., Oreg. State Univ., Corvallis, 1997.

Chang, F.-L., Z. Li, and S. A. Ackerman, Examining the relationship between cloud and radiation quantities derived from satellite observations and model calculations, *J. Clim.*, *13*, 3842–3859, 2000.

Charlson, R. J., J. E. Lovelock, M. O. Andreae, and S. G. Warren, Oceanic phytoplankton, atmospheric sulphur, cloud albedo and climate, *Nature*, *326*, 655–661, 1987.

Coakley, J. A., Jr., and D. G. Baldwin, Towards the objective analysis of clouds from satellite imagery data, *J. Clim. Appl. Meteorol.*, *23*, 1065–1099, 1984.

Coakley, J. A., Jr., R. L. Bernstein, and P. A. Durkee, Effect of ship-stack effluents on cloud reflectivity, *Science*, *237*, 1020–1022, 1987.

Dong, X., T. P. Ackerman, E. E. Clothiaux, P. Pilewskie, and Y. Han, Microphysical and radiative properties of boundary layer stratiform clouds deduced from ground-based measurements, *J. Geophys. Res.*, *102*, 23,829–23,843, 1997.

Downing, H. D., and D. Williams, Optical constants of water in the infrared, *J. Geophys. Res.*, *80*, 1656–1661, 1975.

Duda, D. P., G. L. Stephens, and S. K. Cox, Microphysical and radiative properties of marine stratocumulus from tethered balloon measurements, *J. Appl. Meteorol.*, *30*, 170–186, 1991.

Duynkerke, P. G., H. Zhang, and P. T. Jonker, Microphysical and turbulent structure of nocturnal stratocumulus as observed during ASTEX, *J. Atmos. Sci.*, *52*, 2763–2777, 1995.

Hale, G. M., and M. R. Querry, Optical constants of water in the 200 nm to 200 mm wavelength region, *Appl. Opt.*, *12*, 555–563, 1973.

Han, Q., W. B. Rossow, and A. A. Lacis, Near-global survey of effective droplet radii in liquid water clouds using ISCCP data, *J. Clim.*, *7*, 465–497, 1994.

Han, Q., W. B. Rossow, R. Welch, A. White, and J. Chou, Validation of satellite retrievals of cloud microphysics and liquid water path using observations from FIRE, *J. Atmos. Sci.*, *52*, 4183–4195, 1995.

Hartmann, D. L., M. E. Ockert-Bell, and M. L. Michelsen, The effect of cloud type on the Earth's energy balance: Global analysis, *J. Clim.*, *5*, 1281–1304, 1992.

Kiehl, J. T., Sensitivity of a GCM climate simulation to differences in continental versus maritime cloud drop size, *J. Geophys. Res.*, *99*, 23,107–23,115, 1994.

King, M. D., Y. J. Kaufman, W. P. Menzel, and D. Tanre, Remote-sensing of cloud, aerosol, and water-vapor properties from the Moderate Resolution Imaging Spectrometer (MODIS), *IEEE Trans. Geosci. Remote Sens.*, *30*, 2–27, 1992.

Loeb, N. G., and J. A. Coakley Jr., Inference of marine stratus cloud optical depths from satellite measurements: Does 1D theory apply?, *J. Clim.*, *11*, 215–233, 1998.

Martin, G. M., D. W. Johnson, and A. Spice, The measurement and parameterization of effective radius of drops in warm stratocumulus clouds, *J. Atmos. Sci.*, *51*, 1823–1842, 1994.

Miles, N. L., J. Verlinde, and E. E. Clothiaux, Cloud droplet size distributions in low-level stratiform clouds, *J. Atmos. Sci.*, *57*, 295–311, 2000.

Nakajima, T., and M. D. King, Determination of the optical thickness and effective particle radius of clouds from reflected solar radiation measurements, I, Theory, *J. Atmos. Sci.*, *47*, 1878–1893, 1990.

Nakajima, T. Y., and T. Nakajima, Wide-area determination of cloud microphysical properties from NOAA AVHRR measurements for FIRE and ASTEX regions, *J. Atmos. Sci.*, *52*, 4043–4059, 1995.

Nakajima, T., M. D. King, J. D. Spinhirne, and L. F. Radke, Determination of the optical thickness and effective particle radius of clouds from reflected solar radiation measurements, II, Marine stratocumulus observations, *J. Atmos. Sci.*, *48*, 728–750, 1991.

Nicholls, S., The dynamics of stratocumulus: Aircraft observations and comparisons with a mixed layer model, *Q. J. R. Meteorol. Soc.*, *110*, 783–820, 1984.

Nicholls, S., and J. D. Turton, An observational study of the structure of stratiform cloud sheets, part II, Entrainment, *Q. J. R. Meteorol. Soc.*, *112*, 461–480, 1986.

Platnick, S., Vertical photon transport in cloud remote sensing problems, *J. Geophys. Res.*, *105*, 22,919–22,935, 2000.

Platnick, S., A superposition technique for deriving mean photon scattering statistics in plane-parallel cloudy atmospheres, *J. Quant. Spectrosc. Radiat. Transfer*, *68*, 57–73, 2001a.

Platnick, S., Approximations for horizontal photon transport in cloud remote sensing problems, *J. Quant. Spectrosc. Radiat. Transfer*, *68*, 75–99, 2001b.

Platnick, S., and S. Twomey, Determining the susceptibility of cloud albedo to changes in droplet concentrations with the Advanced Very High Resolution Radiometer, *J. Appl. Meteorol.*, *33*, 334–347, 1994.

Platnick, S., and E. P. J. Valero, A validation study of a satellite cloud retrieval during ASTEX, *J. Atmos. Sci.*, *52*, 2985–3001, 1995.

Rawlins, F., and J. S. Foot, Remotely sensed measurements of stratocumulus properties during FIRE using the C130 aircraft multi-channel radiometer, *J. Atmos. Sci.*, *47*, 2488–2503, 1990.

Rossow, W. B., L. C. Garder, and A. A. Lacis, Global seasonal cloud variations from satellite radiance measurements, part I, Sensitivity of analysis, *J. Clim.*, *2*, 419–458, 1989.

Ryan, R. T., H. H. Blau Jr., P. C. von Thuna, M. L. Cohen, and G. D. Roberts, Cloud microstructure as determined by an optical cloud particle spectrometer, *J. Appl. Meteorol.*, *11*, 149–156, 1972.

Slingo, A., Sensitivity of the Earth's radiation budget to changes in low clouds, *Nature*, *343*, 49–51, 1990.

Slingo, A., R. Brown, and C. L. Wrench, A field study of nocturnal stratocumulus, III, High resolution radiative and microphysical observations, *Q. J. R. Meteorol. Soc.*, *108*, 145–165, 1982.

Stephens, G. L., Radiative effects of clouds and water vapor, in *Global Energy and Water Cycle*, edited by K. A. Browning and R. J. Gurney, pp. 71–90, Cambridge Univ. Press, New York, 1999.

Stephens, G. L., and C. M. R. Platt, Aircraft observations of the radiative and microphysical properties of stratocumulus and cumulus cloud fields, *J. Clim. Appl. Meteorol.*, *26*, 1243–1269, 1987.

Twomey, S., Aerosols, clouds and radiation, *Atmos. Environ.*, *254*, 2435–2442, 1991.

Twomey, S., and T. Cocks, Remote sensing of cloud parameters from spectral reflectance measurements in the near-infrared, *Beitr. Phys. Atmos.*, *62*, 172–179, 1989.

White, A. B., C. W. Fairall, and J. B. Snider, Surface-based remote sensing of marine boundary-layer cloud properties, *J. Atmos. Sci.*, *52*, 2827–2838, 1995.

Wielicki, B. A., R. D. Cess, M. D. King, D. A. Randall, and E. F. Harrison, Mission to Planet Earth: Role of clouds and radiation in climate, *Bull. Am. Meteorol. Soc.*, *76*, 2125–2153, 1995.

───────────────

F.-L. Chang and Z. Li, ESSIC/Department of Meteorology, University of Maryland, 2335 Computer and Science Building, College Park, MD 20742, USA. (zli@atmos.umd.edu)